

Bracing effect mechanism in the collapse of timber-frame houses due to earthquake and snow weight

Junji KIYONO¹ and Aiko FURUKAWA²

¹Department of Urban Management, Kyoto University, Japan

²Department of Civil Engineering, Kyushu University, Japan

(Received for 26 Apr., 2005 and in revised from 15 May, 2006)

ABSTRACT

In this study, a simulation procedure with which the collapse mechanism of a timber-frame house can be traced was developed using the 3-dimensional distinct element method (3D-DEM). The collapse phenomenon of timber-frame houses due to both earthquake and the weight of snow on roofs was simulated, and the effect of diagonal bracing in preventing structures from collapsing was examined. Timber-frame houses with structural elements (columns, beams, floors, foundations, roofs, and diagonal braces) were modeled. The 3D-DEM program was developed introducing rectangular parallelepiped, hexahedral and octahedral elements in order to model these structural elements, and the process of detecting contact between the elements was simplified and made computationally efficient. The difference in collapse behavior between structures that have no diagonal braces, few braces, and many braces was compared using the developed program. The simulated results showed that installing diagonal braces is effective in preventing structures from collapsing due to both earthquake motion and snow weight on roofs. The proposed procedure contributes to providing people with a better understanding of the necessity of repair and reinforcement to avoid catastrophic disaster in coming earthquakes.

1. INTRODUCTION

The Mid-Niigata Prefecture Earthquake, the magnitude of which was 6.8, occurred on October 23rd in 2004. It is reported that more than 10,000 houses collapsed due to this earthquake and, since Niigata is an area of very heavy snowfall, some structures damaged by this earthquake collapsed afterward due to the weight of snow on their roofs (Ministry of Land, 2004). Therefore, we have to consider not only the possibility of structures collapsing due to earthquakes but also the possibility of structures that are leaning or have been damaged by earthquakes collapsing due to the weight of snow on their roofs, and the possibility of the snow on the roofs enlarging the degree of earthquake damage. Repairing and reinforcing the structures as well as removing snow from roofs are important in order to prevent collapse.

We also learned from the 1995 Hyogo-ken Nanbu Earthquake that an important factor that induces structural collapse during earthquakes is the lack of bearing walls, such as diagonal braces and structural walls. It is necessary to increase the yield strength by introducing these diagonal braces and structural walls to prepare for coming great earthquakes. To meet these needs, motivating private users by showing how these bearing walls prevent structural damage in a very understandable manner is important, because users of most timber-frame houses are not public but private.

In this study, the collapse phenomenon of timber houses due to both earthquake and the weight of snow on roofs was simulated,

and the effect of diagonal bracing was examined using the 3-dimensional distinct element method (3D-DEM). The DEM is a numerical analysis technique, in which the positions of elements are calculated by solving equations of motion step by step (Cundall, 1971). Both individual and group behavior can be simulated. The DEM as a tool for numerical simulation has been widely applied to various fields including not only geotechnical engineering (Ohnishi et al., 1986), structural engineering (Meguro et al., 1994) and coastal engineering (Harada et al, 2002), but also social science such as crowd evacuation (Kiyono et al., 1998; Kiyono et al., 2001) and train derailment (Kiyono et al., 2003). The DEM is originally a method for dealing with discontinuum; therefore, joints that connect elements were introduced to deal with continuum. Now that the DEM can treat behavior from continuum to discontinuum, it can trace structural behavior from elastic behavior to large deformation such as half collapse and complete collapse. Using the theoretical background of the DEM developed by Cundall (1971), we created a DEM code to calculate the behavior of timber-frame houses. We originally modeled the structural components such as columns, beams, bracings and roofs as distinct elements, and applied the DEM to timber-frame houses.

In the DEM, a structure is modeled as an assembly of distinct elements connected by virtual springs and dashpots where elements come into contact. Timber-frame houses with structural elements (columns, beams, floors, foundations, roofs, and diagonal braces) were modeled. The 3D-DEM program was developed introducing rectangular parallelepiped, hexahedral and octahedral

elements in order to model these structural elements, and the process of detecting contact between elements was simplified and made computationally efficient.

The difference in collapse behavior between structures that have no diagonal braces, few braces, and many braces was compared using the developed program. The simulated results showed that installing diagonal braces is effective in preventing structures from collapsing due to both earthquake motion and snow weight on roofs. The structures, with some of their column-beam connections and brace-beam connections broken, were also simulated and the results were compared with those of intact structures. It was found that intact brace-beam connections worked effectively to prevent collapse even though some joints broke. Our developed 3D-DEM program succeeded in showing visually the bracing effects to prevent structural collapse, which will motivate users' initiative for reinforcement.

2. ANALYTICAL METHOD

2.1 Equation of Motion

The DEM, a numerical analysis method that computes the position of individual elements by solving equations of motion step by step, was used. All the elements are assumed to be rigid. Virtual springs and dashpots in the normal and tangential directions are generated when an element comes into contact with other elements, and the contact force acts through these generated virtual springs and dashpots. By solving the equation of motion for each element step by step, the behavior of all the elements in a combination can be traced. The motion of a rigid body can be classified as the translational motion of its center of gravity and rotational motion around the center of gravity.

(1) Translational motion of the center of gravity

The forces acting on an element are external force (f_x, f_y, f_z) such as gravity and earthquake motion, the sum of the contact forces between the elements (F_x, F_y, F_z), and the resistance forces of the joints (F_{px}, F_{py}, F_{pz}).

Therefore, accelerations of an element are calculated by:

$$\ddot{x} = (f_x + \sum F_x + \sum F_{px}) / m \quad (1)$$

$$\ddot{y} = (f_y + \sum F_y + \sum F_{py}) / m \quad (2)$$

$$\ddot{z} = (f_z + \sum F_z + \sum F_{pz}) / m \quad (3)$$

in which x, y, z are the coordinates of the center of gravity, subscripts x, y, z , the parameters in the x -, y -, z -direction, m , the element's mass, and Δt , the time increment in the analysis.

Assuming that acceleration is constant for a short period, Δt , the velocity and displacement of the center of gravity of each element can be calculated by means of the following difference scheme, and the total structural behavior can be traced:

$$\begin{Bmatrix} \dot{x}_t \\ \dot{y}_t \\ \dot{z}_t \end{Bmatrix} = \begin{Bmatrix} \dot{x}_{t-\Delta t} \\ \dot{y}_{t-\Delta t} \\ \dot{z}_{t-\Delta t} \end{Bmatrix} + \begin{Bmatrix} \ddot{x}_{t-\Delta t} \\ \ddot{y}_{t-\Delta t} \\ \ddot{z}_{t-\Delta t} \end{Bmatrix} \Delta t \quad (4)$$

$$\begin{Bmatrix} x_t \\ y_t \\ z_t \end{Bmatrix} = \begin{Bmatrix} x_{t-\Delta t} \\ y_{t-\Delta t} \\ z_{t-\Delta t} \end{Bmatrix} + \begin{Bmatrix} \dot{x}_{t-\Delta t} \\ \dot{y}_{t-\Delta t} \\ \dot{z}_{t-\Delta t} \end{Bmatrix} \Delta t \quad (5)$$

(2) Rotational motion around the center of gravity

Here, we consider two frames of reference, the absolute frame of reference and the element frame of reference. The absolute frame of reference (x, y, z) stated here is a system that has its origin at the center of gravity. The element frame of reference (ξ, η, ζ) stated here is a system whose coordinate axes are inertia axes and whose origin is the center of gravity.

Rotation around its center of gravity is obtained from Euler's equations of motion. The equations for the ξ -, η -, and ζ -directions are

$$I_\xi \frac{d\omega_\xi}{dt} - (I_\eta - I_\zeta) \omega_\eta \omega_\zeta = (\sum_i r_i \times F_i)_\xi \quad (6)$$

$$I_\eta \frac{d\omega_\eta}{dt} - (I_\xi - I_\zeta) \omega_\xi \omega_\zeta = (\sum_i r_i \times F_i)_\eta \quad (7)$$

$$I_\zeta \frac{d\omega_\zeta}{dt} - (I_\xi - I_\eta) \omega_\xi \omega_\eta = (\sum_i r_i \times F_i)_\zeta \quad (8)$$

in which ξ, η , and ζ are the inertia axes of the coordinates, and I_i and ω_i ($i = \xi, \eta, \zeta$), respectively, are the moments of inertia and rotational velocities around the center of gravity in the element frame of reference. r_i denotes the coordinate vector of a vertex of a rigid body, and F_i denotes the force vector affecting the vertex in the absolute frame of reference.

The angular velocity in the element frame of reference, $\omega_\xi, \omega_\eta, \omega_\zeta$, can be obtained using the angular velocity in the previous step and the angular acceleration obtained from Eqs. (6), (7) and (8) as

$$\begin{Bmatrix} \omega_{\xi,t} \\ \omega_{\eta,t} \\ \omega_{\zeta,t} \end{Bmatrix} = \begin{Bmatrix} \omega_{\xi,t-\Delta t} \\ \omega_{\eta,t-\Delta t} \\ \omega_{\zeta,t-\Delta t} \end{Bmatrix} + \begin{Bmatrix} \dot{\omega}_{\xi,t-\Delta t} \\ \dot{\omega}_{\eta,t-\Delta t} \\ \dot{\omega}_{\zeta,t-\Delta t} \end{Bmatrix} \Delta t \quad (9)$$

The angular velocity in the absolute frame of reference, $\omega_x, \omega_y, \omega_z$, can be obtained by the following transformation

$$\omega_x = \lambda_x \omega_\xi + \mu_x \omega_\eta + \nu_x \omega_\zeta \quad (10)$$

$$\omega_y = \lambda_y \omega_\xi + \mu_y \omega_\eta + \nu_y \omega_\zeta \quad (11)$$

$$\omega_z = \lambda_z \omega_\xi + \mu_z \omega_\eta + \nu_z \omega_\zeta \quad (12)$$

where λ_x, μ_x, ν_x are the direction cosine of the x -axis (cosine between the x -axis and the ξ -, η -, ζ -axes), λ_y, μ_y, ν_y , the direction cosine of the y -axis, and λ_z, μ_z, ν_z , the direction cosine of the z -axis.

Velocity at an arbitrary point in the rigid body, $r = (r_x, r_y, r_z)$, is obtained as the outer product between the angular velocity vector and coordinate vector as

$$\begin{Bmatrix} \dot{r}_x \\ \dot{r}_y \\ \dot{r}_z \end{Bmatrix} = \begin{Bmatrix} \omega_x \\ \omega_y \\ \omega_z \end{Bmatrix} \times \begin{Bmatrix} r_x \\ r_y \\ r_z \end{Bmatrix} \quad (13)$$

By integrating the obtained velocity, the coordinate of the point is obtained from the following difference scheme.

$$\begin{Bmatrix} r_{x,t} \\ r_{y,t} \\ r_{z,t} \end{Bmatrix} = \begin{Bmatrix} r_{x,t-\Delta t} \\ r_{y,t-\Delta t} \\ r_{z,t-\Delta t} \end{Bmatrix} + \begin{Bmatrix} \dot{r}_{x,t-\Delta t} \\ \dot{r}_{y,t-\Delta t} \\ \dot{r}_{z,t-\Delta t} \end{Bmatrix} \Delta t \quad (14)$$

Since distinct elements are modeled using rectangular parallelepipeds, hexahedrons and octahedrons in this paper, we take r as the coordinate of the vertex.

As explained above, the 3-dimensional behavior of each distinct element can be calculated, and the structural behavior can be obtained as an assembly of the behavior of all elements.

2.2 Contact Evaluation

When elements come into contact, springs and dashpots are generated in the calculation (Fig. 1). Evaluation of contact is made by considering the collocation between the two elements concerned. To simplify and make time-efficient the process of detecting contact, we assume the vertex of the rectangular parallelepiped to be 1/8 of a circle, and the edge to be 1/4 of a circular cylinder as shown in Fig. 2. A similar assumption was made regarding hexahedron and octahedron elements. By introducing this assumption, the patterns of contact are classified into 4 patterns: contact between vertexes, contact between a vertex and an edge, contact between a vertex and a face, and contact between edges as shown in Fig. 3. Figure 3 shows the contact between the vertex and face of two elements, and the virtual springs and dashpots generated between these elements. By assuming small values for the radius of the circle and the circle cylinder, the first two contact patterns,

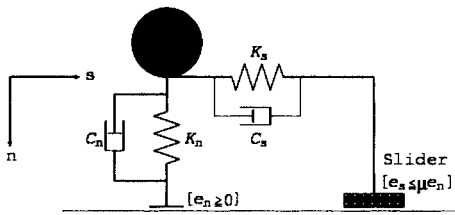


Fig. 1 Contact model of elements

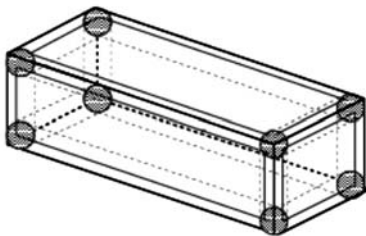


Fig. 2 Rectangular parallelepiped model

contact between vertexes and contact between a vertex and an edge, can be ignored. These assumptions are also effective in solving the instability phenomenon that occurs in contact between a sharp vertex and another sharp vertex or an edge. In this study, we adopted 10% of the edge length of the least edge for the value of the radius, r .

2.3 Contact force

Increments in the restoring and damping forces in the normal and tangential directions (Δe_n , Δe_s , Δd_n , Δd_s) for interval Δt are expressed by the increments of relative displacement in these directions, Δn and Δs :

$$\Delta e_n = K_n \Delta n \quad (15)$$

$$\Delta e_s = K_s \Delta s \quad (16)$$

$$\Delta d_n = C_n \Delta n / \Delta t \quad (17)$$

$$\Delta d_s = C_s \Delta s / \Delta t \quad (18)$$

in which K_n and K_s , and C_n and C_s , respectively, are the spring constants and damping coefficients in the normal and tangential directions. The restoring and damping forces in each direction ($[e_n]_t$, $[e_s]_t$, $[d_n]_t$, $[d_s]_t$) at arbitrary time t are obtained from the preceding equations:

$$[e_n]_t = [e_n]_{t-\Delta t} + \Delta e_n \quad (19)$$

$$[e_s]_t = [e_s]_{t-\Delta t} + \Delta e_s \quad (20)$$

$$[d_n]_t = \Delta d_n \quad (21)$$

$$[d_s]_t = \Delta d_s \quad (22)$$

When the restoring force exceeds the friction limit, the tangential force is governed by dynamic friction. The total contact forces in both directions are:

$$[F_n]_t = [e_n]_t + [d_n]_t \quad (23)$$

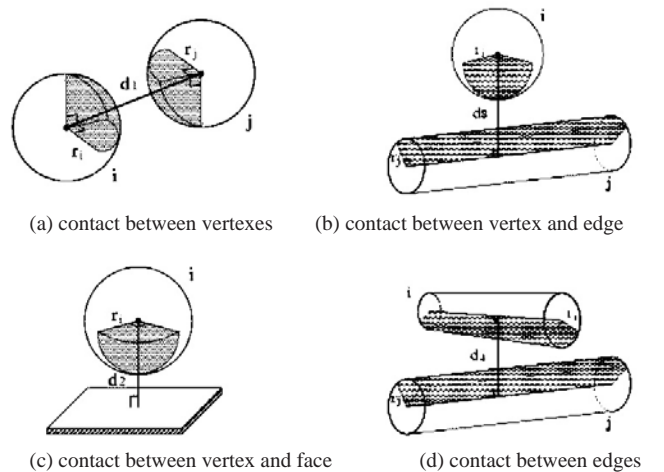


Fig. 3 Contact patterns

$$[F_s]_t = [e_s]_t + [d_s]_t \quad (24)$$

Forces F_x , F_y and F_z , in Eqs. (1), (2) and (3) are obtained by combining the above forces in the target direction.

2.4 Resistance force at joint

Increments in the resistance forces in the normal and tangential directions (Δe_{pn} , Δe_{ps} , Δd_{pn} , Δd_{ps}) for interval Δt are expressed by the increments of relative displacement in these directions, Δn and Δs :

$$\Delta e_{pn} = K_{pn} \Delta n \quad (25)$$

$$\Delta e_{ps} = K_{ps} \Delta s \quad (26)$$

$$\Delta d_{pn} = C_{pn} \Delta n / \Delta t \quad (27)$$

$$\Delta d_{ps} = C_{ps} \Delta s / \Delta t \quad (28)$$

in which K_{pn} and K_{ps} , and C_{pn} and C_{ps} , respectively, are the spring constants and damping coefficients in the normal and tangential directions of joints. The resistance forces in each direction ($[e_{pn}]_t$, $[e_{ps}]_t$, $[d_{pn}]_t$, $[d_{ps}]_t$) at arbitrary time t are obtained from the preceding equations:

$$[e_{pn}]_t = [e_{pn}]_{t-\Delta t} + \Delta e_{pn} \quad (29)$$

$$[e_{ps}]_t = [e_{ps}]_{t-\Delta t} + \Delta e_{ps} \quad (30)$$

$$[d_{pn}]_t = \Delta d_{pn} \quad (31)$$

$$[d_{ps}]_t = \Delta d_{ps} \quad (32)$$

When the resistance force exceeds the limit, P_{max} , the joint is broken and it can no longer sustain any force. The total resistance forces in both directions are:

$$[F_{pn}]_t = [e_{pn}]_t + [d_{pn}]_t \quad (33)$$

$$[F_{ps}]_t = [e_{ps}]_t + [d_{ps}]_t \quad (34)$$

3. PARAMETERS AND ANALYTICAL MODEL

3.1 Contact parameters

(1) Contact parameters for structural elements

In the DEM, most of the force-displacement laws for elastic contact between two spherical elements in the normal direction are based on the Hertz theory (Johnson, 1985). Imagine that two spherical elements, i and j , are in contact and subjected to a normal contact force. Assume r_i and r_j to be the radii of the two elements. Young's modulus for the elements are E_i and E_j , and Poisson's ratios are ν_i and ν_j . The equivalent Young's modulus, E , is

$$E = \left(\frac{1-\nu_i^2}{E_i} + \frac{1-\nu_j^2}{E_j} \right)^{-1} \quad (35)$$

and the relative radius of contact curvature, r , is

$$r = \left(\frac{1}{r_i} + \frac{1}{r_j} \right)^{-1} \quad (36)$$

According to the Hertz theory of the elastic contact of two spheres in the normal direction, the force-displacement relationship is

$$[e_n]_t = \frac{4}{3} E \sqrt{r \cdot n^3} \quad (37)$$

where $[e_n]_t$ and n , respectively, are the normal contact force and contact displacement at time t . This force-displacement relationship can be transformed into the differential equation

$$[e_n]_t = [e_n]_{t-\Delta t} + 2E\sqrt{r \cdot n} \Delta n \quad (38)$$

where Δn is the increment of contact displacement. The spring constant in the normal direction at time t is therefore expressed as

$$K_n = 2E\sqrt{r \cdot n} \quad (39)$$

Because this study uses rectangular parallelepiped elements, we utilized an equivalent radius that has the same volume.

The spring constant in the tangential direction was defined as

$$K_s = \frac{K_n}{2(1+\nu)} \quad (40)$$

where ν is Poisson's ratio for the timber frame.

As for the damping coefficient, critical damping was adopted:

$$C_n = 2\sqrt{mK_n} \quad (41)$$

$$C_s = 2\sqrt{mK_s} \quad (42)$$

where m is the equivalent mass of two elements. When their masses are m_i and m_j ,

$$m = \left(\frac{1}{m_i} + \frac{1}{m_j} \right)^{-1} \quad (43)$$

These parameters are calculated by the use of Young's modulus of timber, 90×10^3 kgf/cm², and a Poisson's ratio of 0.4 (Architectural Institute of Japan, 1995).

In fact, Young's modulus of timber is different in two directions: the fibrous direction and its perpendicular direction. Young's modulus in the fibrous direction is larger than that in its perpendicular direction. However, we do not consider the anisotropy of timber in this study, and used Young's modulus in the fibrous direction because timber-frame houses are designed to use the strength of timber in the fibrous direction.

(2) Contact parameters for snow

We assumed the contact parameters for snow (K_n , K_s , C_n , C_s) to be proportional to the element mass because reaction force due to contact becomes larger as the density of snow increases by

tamping. As for the damping coefficient, critical damping was adopted.

In this study, the value of the contact parameters for snow is the same in the normal and tangential directions, even though those for structures are different in two directions. It is based on the assumption that snow is a mass of isotropic crystals, and using different contact parameters in two directions is not appropriate because we model snow using rectangular parallelepipeds for convenience.

3.2 Joint Parameters

In the usual DEM, connectivity between elements is not considered, with the elements acting independently as a discontinuum. The columns, beams and braces of a real structure, however, are connected by joints, and the structure acts as a continuum. Joints, which allow a structure to behave as a continuum until its joints are broken, are therefore introduced.

Increasing the amount of bearing wall is important but not sufficient in strengthening a structure. Increasing the strength of joints is also necessary. Lessons from the 1995 Hyogo-ken Nambu Earthquake showed that a major factor in the collapse of many timber-frame houses is the weakness of joints.

As for old timber houses, clamps were used for connecting columns and nails were used for connecting braces. As for recent timber houses, auxiliary metal fittings such as corner metal fittings and angle plates are used at the joint parts of tenons connecting columns and beams, and bracing plates are used to connect braces and beams. In this study, we assumed joints at column-beam connections to be modeled using corner metal fittings, and joints at brace-beam connections to be modeled using bracing plates.

Joints resist not only tension force but also compression force. When two elements connected by a joint are in contact with each other, both contact force and resistance force work at the same time.

(1) Joint parameters for column-beam connection

Joint parameters for column-beam connections (K_{pn} , K_{ps} , C_{pn} , C_{ps} , P_{max}) were obtained from the threshold intensity of the corner metal fitting shown in **Fig. 4 (a)**. According to the Japan Housing & Wood Technology Center (Japan Housing & Wood technology Center, 2001), the yield strength is published as $P_{max} = 600 \text{ kgf} = 600 \times 9.8 \text{ N} = 5880 \text{ N}$. In this study, it is assumed that metal fittings are attached to columns with a length of about 10 cm. It was also assumed that the metal fittings break when the column and beam concerned are separated 10 cm from

the contact point, meaning that the spring modeling joint is lengthened by 10 cm. Therefore, the spring constant for the both normal and tangential directions was obtained by dividing the yield strength by a length of 10 cm, as $K_{pn} = K_{ps} = 5880 \text{ N}/0.1 \text{ m} = 58800 \text{ N/m}$. We assumed that the damping coefficient for the joint is 0.0 in both the normal and tangential directions. Joints break when the restoring force exceeds the joint intensity.

(2) Joint parameters for brace-beam connection

Joint parameters for brace-beam connections (K_{pn} , K_{ps} , C_{pn} , C_{ps} , P_{max}) were obtained from the threshold intensity of the bracing plate shown in **Fig. 4 (b)**. According to the Japan Housing & Wood Technology Center (2001), the yield strength is published as $P_{max} = 710 \text{ kgf} = 710 \times 9.8 \text{ N} = 6958 \text{ N}$. In this study, it is assumed that the bracing plates are attached to braces with a length of about 10 cm. It was also assumed that the bracing plates break when the column and beam concerned are separated 10 cm from the contact point, meaning that the spring modeling joint is lengthened by 10 cm. Therefore, the spring constant for both normal and tangential directions was obtained by dividing the yield strength by a length of 10 cm, as $K_{pn} = K_{ps} = 6958 \text{ N}/0.1 \text{ m} = 69580 \text{ N/m}$. We assumed that the damping coefficient for the joint is 0.0 in both the normal and tangential directions. Joints break when the restoring force exceeds the joint intensity.

The contact parameters for structures and snow, and the joint parameters used are shown in **Table 1**. When elements are in contact, it is assumed that spring contacts and dashpots are serially connected. The $P-\delta$ effect is automatically taken into account in the DEM.

3.3 Interval

The interval used for computation markedly affects the stability of the results. If it is too long, the results will diverge. Cundall

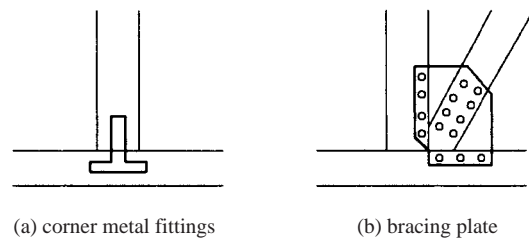


Fig. 4 auxiliary metal fittings

Table 1. Contact and joint parameters

	Contact parameters for structures	Contact parameters for snow (1/kg)	Joint parameters for column-beam connection	Joint parameters for brace-beam connection
K_n (N/m)	$2E\sqrt{r \cdot n}$	3.948×10^4	5.880×10^4	6.958×10^4
K_s (N/m)	$\frac{K_n}{2(1+\nu)}$	3.948×10^4	5.880×10^4	6.958×10^4
C_n (Nsec/m)	$2\sqrt{mK_n}$	$2\sqrt{mK_n}$	0.0	0.0
C_s (Nsec/m)	$2\sqrt{mK_s}$	$2\sqrt{mK_s}$	0.0	0.0

(1971) recommends the following interval:

$$\Delta t < 2\sqrt{m / K_n} \quad (44)$$

From the above equation, the limitation is $<1.0 \times 10^{-3}$ (sec). We chose to use an interval of $=1.0 \times 10^{-5}$ (sec).

3.4 Analytical model

(1) Modeling of structures

The structures analyzed are two-story timber-frame houses. Calculations of the mass and moments of inertia of these elements are based on the density of the Japanese cypress (0.34 g/cm^3). There are three models, A, B, and C. Their 3-D views, front views, and side views are shown respectively in Figs. 5, 6, 7. The

difference in these three models is the number of diagonal braces. The structures are 8.34 m wide, 7.43 m deep, and 7.5 m high. Each floor is 2.73 m high. The entrance is 1.812 m wide and 3.76 m deep. All columns are modeled by rectangular parallelepipeds. The 18 columns with a width of 12 cm and a height of 2.73 m are placed in total (9 columns in each floor). The 72 columns with a width of 10.5 cm and a height of 2.73 m are placed in total (33 columns in each floor, 6 in the entrance). Beams, floors and foundations are also modeled by rectangular parallelepipeds, and have a depth of 12 cm, 20 cm and 30 cm, respectively. Roofs are modeled using two hexahedrons and two octahedrons of 12 cm wide. Diagonal braces are modeled using octahedrons that have a width of 9 cm, a depth of 4.5 cm and a height of 2.73 m. The mass and

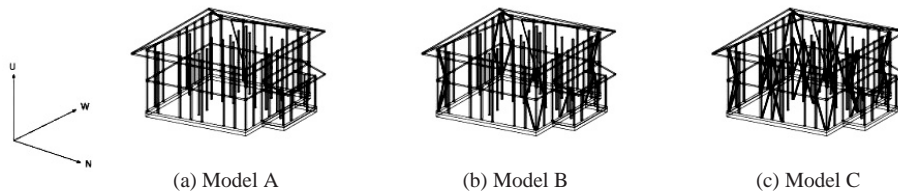


Fig. 5 Analytical models (3D view)

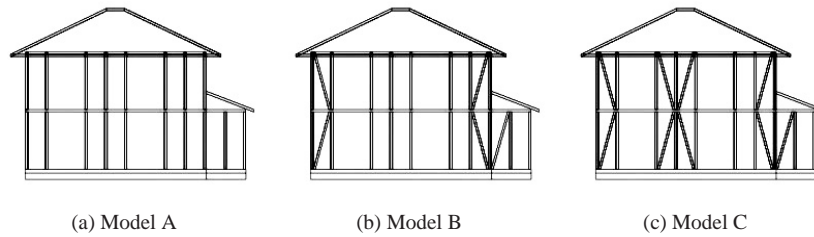


Fig. 6 Analytical models (front view)

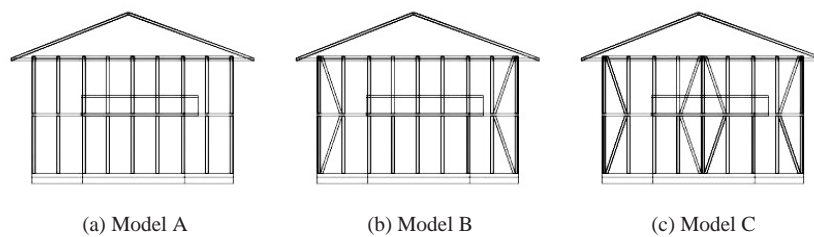


Fig. 7 Analytical models (side view)

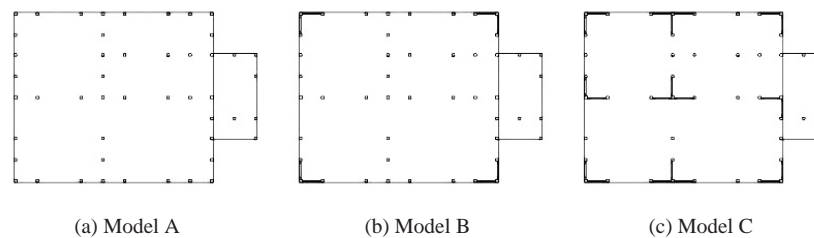


Fig. 8 Arrangement drawing of the first floor

inertia moment for each element are calculated using its volume and a density of 0.34 g/cm^3 . The weight of the finishing material is not considered.

The layout drawing of the columns and braces on the first floor for three models are shown in Fig. 8. The arrangement on the second floor is the same as that of the first floor except that the second floor has no entrance. Model A has no diagonal braces, Model B has 16 braces in the four corners (8 braces on each floor), and Model C has 44 braces (21 braces on each floor and 2 at the entrance).

(2) Modeling of snow

To simulate the collapse phenomenon of structures due to the weight of snow on their roofs, elements modeling snow were introduced. It is assumed that snow acts as clumps that are cumulated and tamped. The snow was modeled using two hexahedrons and two octahedrons that have the same section area as that of the roofs and with a width of 100 cm.

The density of the cumulated snow in Niigata is about $70\text{-}90 \text{ kg/m}^3$, which is heavier than that in Hokkaido and Tohoku District, $50\text{-}80 \text{ kg/m}^3$. The condition of snow varies widely due to temperature and sunshine, and snow in areas where the tempera-

ture in the afternoon exceeds 0°C has a tendency to be greater, being melted and re-tamped. Considering these facts, this study adopted the upper value, 90 kg/m^3 , as the snow density. According to the Japanese building code, the design load for snow is 300 kg/m^3 , which is heavier than the density used in the analysis. We did not use the design load to model the realistic situation.

4. RESULTS

Acceleration records obtained at Ojiya Observatory of Kyoshin-Net managed by the National Research Institute for Disaster Prevention were used with the modeled structures (Fig. 9).

As for the collapse mechanism, only resistance force at joints is considered. Buckling of columns and braces, and bending fracture of columns are ignored. A joint consists of four springs, and these springs are located at four corners of the contact area. Each spring can only resist compression and tension force and does not have any resistance against bending moment. However, the joints have resistance against the bending moment by a combination of four springs.

The findings were as follows.

4.1 Structural behavior due to earthquake

First, the collapse behavior of Models A, B, C, which are

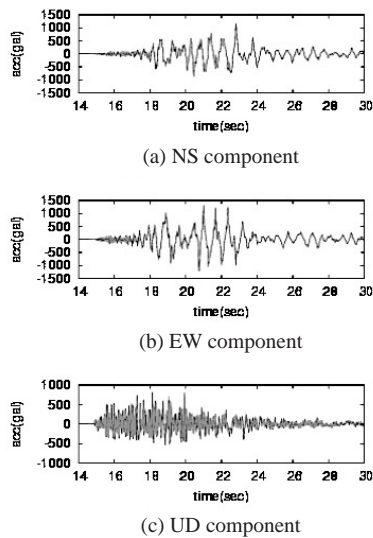


Fig. 9 Input ground motion

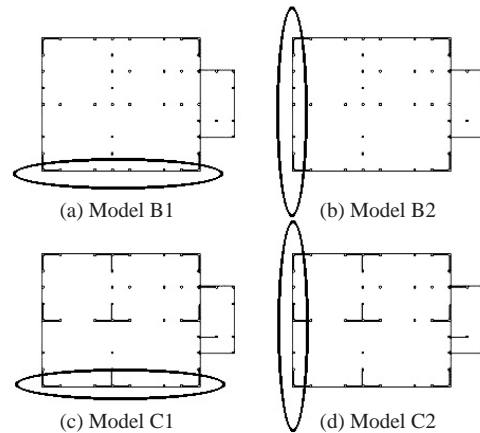


Fig. 10 Damaged joints

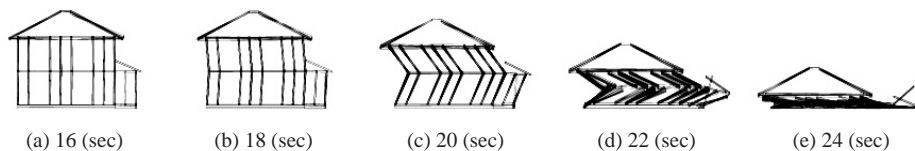


Fig. 11 Collapse behavior of Model A due to earthquake (front view)

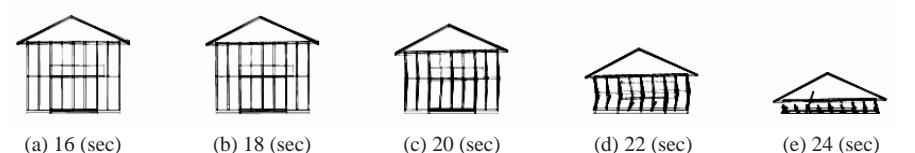


Fig. 12 Collapse behavior of Model A due to earthquake (side view)

affected by the input ground motion shown in **Fig. 9**, was simulated.

(1) Behavior of Model A

The collapse behavior of Model A is shown in **Figs. 11, 12**. The structures started tilting in the south-north direction at about 18 seconds when the acceleration increased, and completely collapsed at 24 seconds. It was found that resistance to lateral force due to the earthquake was very small because Model A has no diagonal braces.

(2) Behavior of Model B

The seismic behavior of Model B is shown in **Figs. 13, 14**. Model B did not collapse because it has 18 diagonal braces, which resisted lateral force due to the earthquake. By comparing the side view of Models A (**Fig. 11**) and B (**Fig. 13**), the effect of braces is

clear; they prevent a structure from collapsing using its resistance both to compression and tension.

(3) Behavior of Model C

The seismic behavior of Model C is shown in **Figs. 15, 16**. Model C did not collapse because it has 44 diagonal braces, which resisted lateral force due to the earthquake.

4.2 Structural behavior due to the weight of snow

Secondly, the collapse behavior of Models A, B, C, which are affected by the weight of snow on their roofs, was simulated.

(1) Behavior of Model A

The collapse behavior of Model A is shown in **Figs. 17, 18**. Due to the heavy snow, Model A started tilting as soon as the

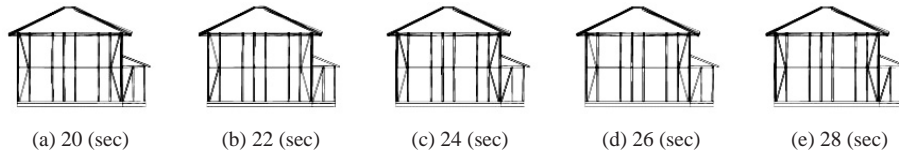


Fig. 13 Collapse behavior of Model B due to earthquake (front view)

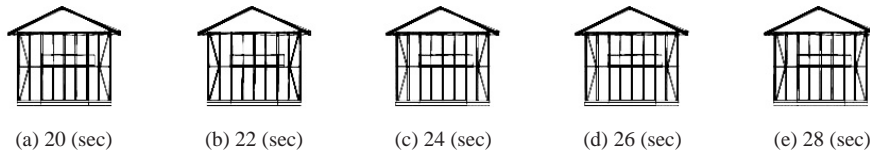


Fig. 14 Collapse behavior of Model B due to earthquake (side view)

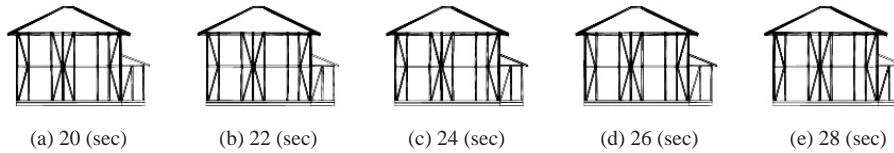


Fig. 15 Collapse behavior of Model C due to earthquake (front view)

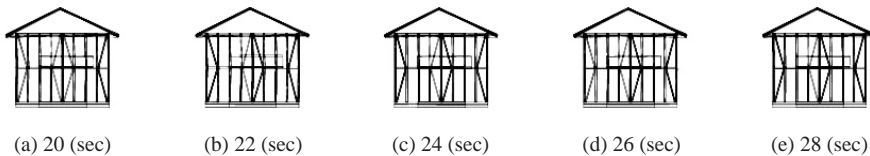


Fig. 16 Collapse behavior of Model C due to earthquake (side view)

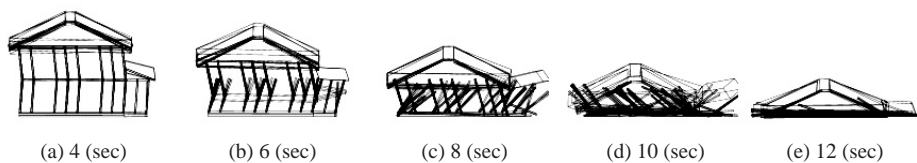


Fig. 17 Collapse behavior of Model A due to snow weight (front view)

analysis began and completely collapsed at 12 seconds. Model A has less resistance both to vertical and lateral forces. Therefore, once it tilted a little, it started to collapse due to the heavy snow.

(2) Behavior of Model B

Model B did not collapse due to the weight of snow because the model is strengthened by bracings. This model stood still, and figures describing the behavior of Model B are therefore omitted. The effect of bracing is apparent.

(3) Behavior of Model C

Model C did not collapse due to the weight of snow because the model is strengthened by bracings. This model stood still, and figures describing the behavior of Model C are therefore omitted. The effect of bracing is apparent.

4.3 Behavior of damaged structures due to earthquake

Next, the seismic behavior of damaged structures was simulated. We assumed two damaged cases for both Models B and C, and named them B1, B2 and C1, C2.

(1) Damage models

a) Model B1

Model B1 is the damage model for Model B. Ten joints on the first floor on the east side (the joints framed by the ellipse in Fig. 10 (a)) are broken. Eight joints are column-beam connections and 2 joints are brace-beam connections.

b) Model B2

Model B2 is the damage model for Model B. Ten joints on the first floor on the south side (joints framed by the ellipse in Fig. 10 (b)) are broken. Eight joints are column-beam connections and 2 joints are brace-beam connections.

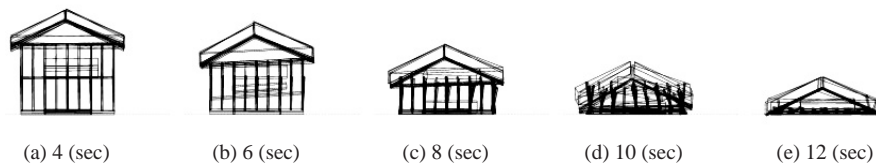


Fig. 18 Collapse behavior of Model A due to snow weight (side view)

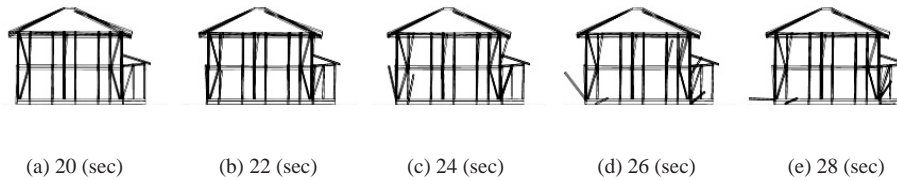


Fig. 19 Collapse behavior of Model B1 due to earthquake (front view)

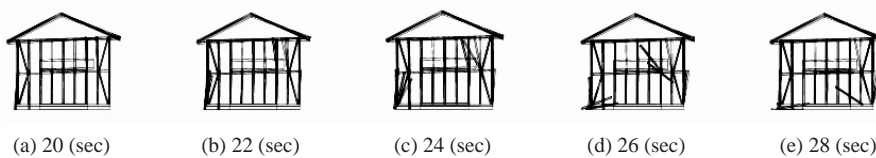


Fig. 20 Collapse behavior of Model B1 due to earthquake (side view)

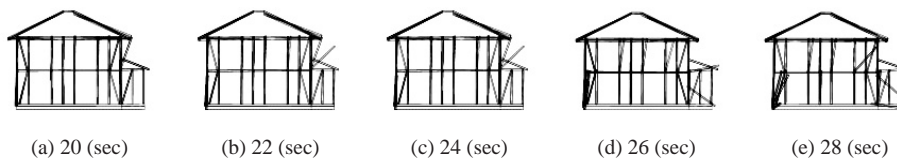


Fig. 21 Collapse behavior of Model B2 due to earthquake (front view)

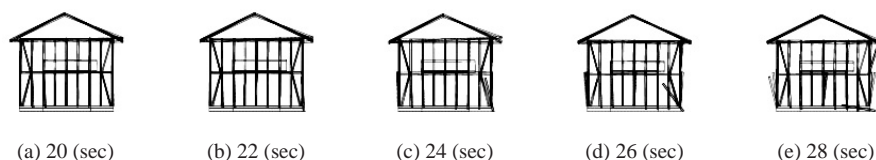


Fig. 22 Collapse behavior of Model B2 due to earthquake (SIDE VIEW)

c) Model C1

Model C1 is the damage model for Model C. Twelve joints on the first floor on the east side (joints framed by the ellipse in Fig. 10 (c)) are broken. Eight joints are column-beam connections and 4 joints are brace-beam connections.

d) Model C2

Model C2 is the damage model for Model C. Eleven joints on the first floor on the south side (joints framed by the ellipse in Fig. 10 (c)) are broken. Eight joints are column-beam connections and 3 joints are brace-beam connections.

(2) Behavior of Model B1

The seismic behavior of Model B1 is shown in Figs. 19, 20. Because the joints on the first floor on the east side (the near side in Fig. 19 and the left-hand side in Fig. 20) are broken, Model B1 swayed greatly in the east-west direction (Fig. 20). As shown in Fig. 19 (e), it was found that the column-beam connections on the first floor on the west side (the right-hand side in Fig. 19) broke but the brace-beam connections did not break, and we succeeded in simulating these intact joints of braces supporting the structure and preventing it from collapsing.

(3) Behavior of Model B2

The seismic behavior of Model B2 is shown in Figs. 21, 22.

Because the joints on the first floor on the south side (the left-hand side in Fig. 21 and the rear in Fig. 22) are broken, Model B2 swayed in the south-north direction (Fig. 21). As shown from the comparison between Fig. 19 and Fig. 21, Model B2 whose joints on the south side are broken are more significantly damaged in the south-north direction and less damaged in the east-west direction than Model B1 whose joints on the east side are broken.

(4) Behavior of Model C1

The seismic behavior of Model C1 is shown in Figs. 23, 24. Because the joints on the first floor on the east side (the near side in Fig. 23 and the left-hand side in Fig. 24) are broken, Model C1 swayed in the east-west direction (Fig. 23). By comparing the behavior of models B1 (Fig. 20) with that of Model C1 (Fig. 23), it was found that the deformation of Model C1 with more braces was less than that of Model B1. The effect of braces is clear.

(5) Behavior of Model C2

The seismic behavior of Model C2 is shown in Figs. 25, 26. Although the joints on the first floor on the south side (the left-hand side in Fig. 25 and the rear in Fig. 26) are broken, the structure is very stable in both the south-north and east-west directions. One reason for this is that the maximum peak acceleration in the south-north direction is smaller than that in the east-west direction,

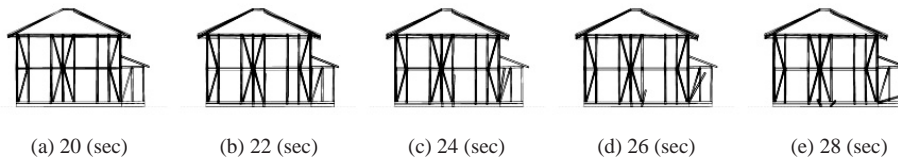


Fig. 23 Collapse behavior of Model C1 due to earthquake (front view)

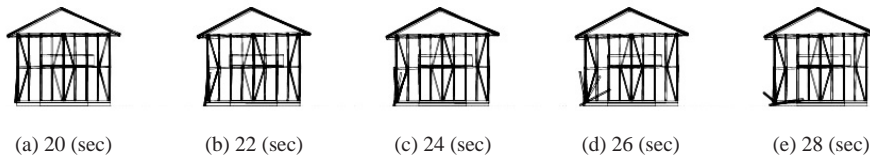


Fig. 24 Collapse behavior of Model C1 due to earthquake (side view)

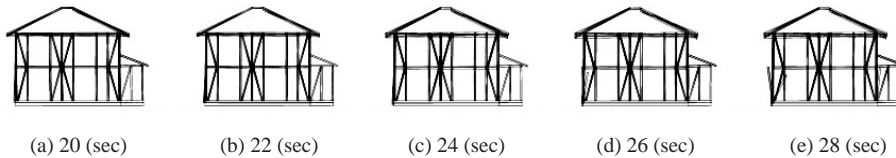


Fig. 25 Collapse behavior of Model C2 due to earthquake (front view)

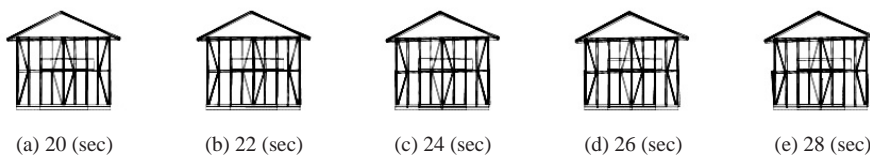


Fig. 26 Collapse behavior of Model C2 due to earthquake (side view)

and another reason is that more braces are placed in the south-north direction.

4.4 Behavior of damaged structures due to both earthquake and snow weight

Lastly, the collapse behavior of damaged structures due to both earthquake and snow weight was simulated.

(1) Behavior of Model B1

The collapse behavior of Model B1 is shown in **Figs. 27, 28**. Because the joints on the first floor on the east side (the near side in **Fig. 27** and the left-hand side in **Fig. 28**) are broken, Model B1 swayed largely in the east-west direction (**Fig. 28**). The structure did not collapse, but more columns fell, the structure leaned more due to the weight of snow on the roofs, and more damage occurred than in the cases with no snow (**Figs. 19, 20**).

(2) Behavior of Model B2

The collapse behavior of Model B2 is shown in **Figs. 29, 30**. Because the joints on the first floor on the south side (the left-hand side in **Fig. 29** and the rear in **Fig. 30**) are broken, Model B2 swayed in the south-north direction (**Fig. 29**). More damage occurred than in the cases with no snow (**Figs. 21, 22**).

(3) Behavior of Model C1

The seismic behavior of Model C1 is shown in **Figs. 31, 32**. Because the joints on the first floor on the east side (the near side in **Fig. 31** and the left-hand side in **Fig. 32**) are broken, Model C1 swayed in the east-west direction (**Fig. 32**). It was found that more damage occurs due to snow through comparison with cases with no snow (**Figs. 23, 24**), and it was also found that the severity of the damage to Model C1 was smaller than that of Model B1 from the comparison with Model B1 (**Figs. 27, 28**), showing that braces

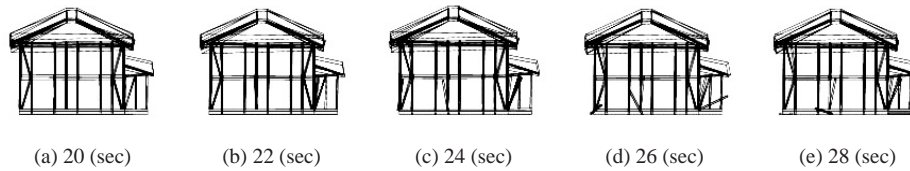


Fig. 27 Collapse behavior of Model B1 due to earthquake and snow weight (front view)

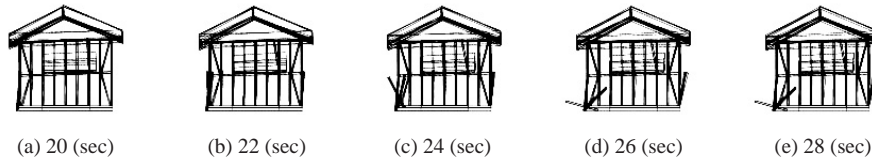


Fig. 28 Collapse behavior of Model B1 due to earthquake and snow weight (side view)

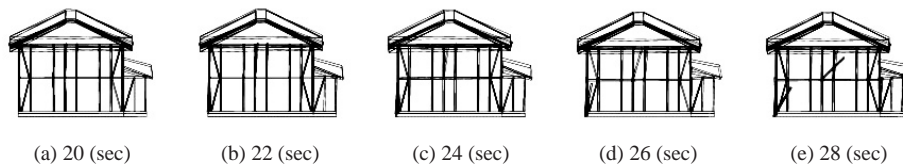


Fig. 29 Collapse behavior of Model B2 due to earthquake and snow weight (front view)

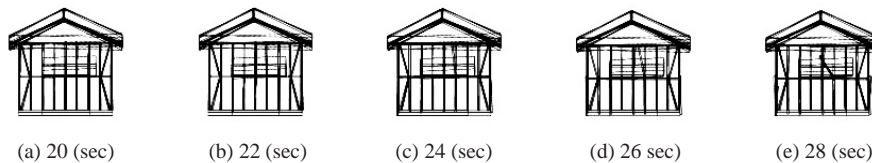


Fig. 30 Collapse behavior of Model B2 due to earthquake and snow weight (side view)

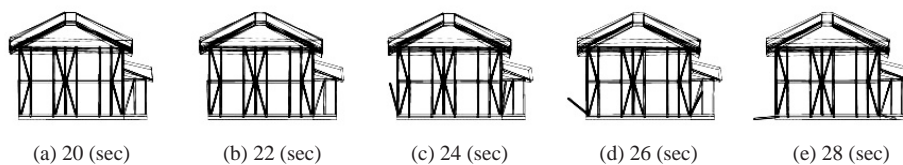


Fig. 31 Collapse behavior of Model C1 due to earthquake and snow weight (front view)

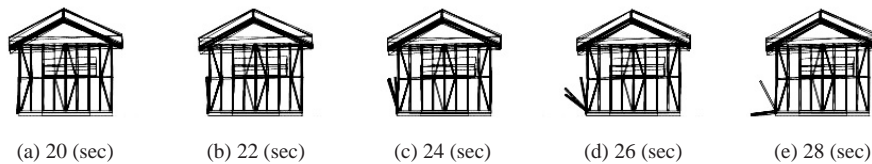


Fig. 32 Collapse behavior of Model C1 due to earthquake and snow weight (side view)

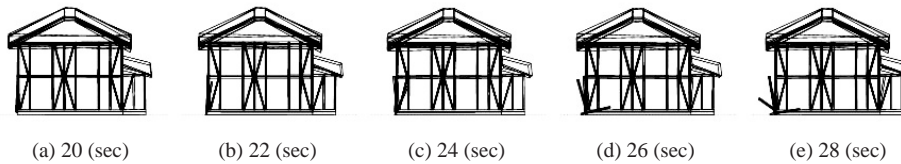


Fig. 33 Collapse behavior of Model C2 due to earthquake and snow weight (front view)

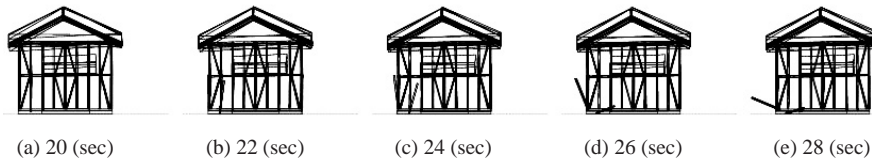


Fig. 34 Collapse behavior of Model C2 due to earthquake and snow weight (side view)

work effectively.

(4) Behavior of Model C2

The collapse behavior of Model C2 is shown in **Figs. 33, 34**. Due to the weight of snow, the second floor leaned more than the cases with no snow (**Figs. 25, 26**). The magnitude of damage to Model C2 is apparently smaller than that of Model B2 from the comparison with Model B2 (**Figs. 29, 30**), showing that braces work effectively.

5. CONCLUSIONS

In this study, a simulation procedure with which the collapse mechanism and the bracing effect of a timber-frame house can be traced was proposed. An analytical program of the proposed procedure is developed based on the 3-dimensional distinct element method (3D-DEM), which is an analytical method for discontinuum. The developed program can deal with rectangular parallelepipeds, hexahedrons, and octahedrons to model structural components such as columns, beams, floors, foundations, roofs, and diagonal braces. The procedure of detecting contact between elements was simplified and made time-efficient. To deal with structural behavior from continuum to discontinuum, a structural joint model was introduced.

We applied the developed program to two-story timber-frame structures with no braces, with few braces, and with many braces, and demonstrated visually the collapse mechanism and the effect of braces against earthquake motion and the weight of snow on roofs.

Collapse patterns vary with the number of diagonal braces that

can resist the lateral loading of the earthquake. If the number of braces is sufficient, a structure will resist an earthquake, even one as severe as the 2004 Mid-Niigata Prefecture Earthquake.

We succeeded in visually showing that installing diagonal braces in a structure is very effective in preventing the structure from collapsing due to both earthquake and snow.

We also were successful in demonstrating that snow on roofs potentially causes more damage to a structure during an earthquake, and pointed out the importance of installing braces as well as removing snow.

By using the developed procedure, we can provide information on whether a damaged or aged structure can avoid collapse just by installing braces or increasing the strength of the joints in a very easily understandable manner. This information gives people the initiative to repair and reinforce their own houses.

Case studies alone are insufficient, more relevant analyses being required, but the methodology presented here should contribute to providing people with a better understanding of the necessity of repair and reinforcement to avoid catastrophic disaster in coming earthquakes.

ACKNOWLEDGMENTS

Partial financial support for this study was provided by the Japan Science and Technology Corporation.

We used the strong motion data by K-net operated by the National Research Institute for Earth Science and Disaster Prevention.

REFERENCES

- Cundall, P.A., 1971. A computer model for simulating progressive, large-scale movements in blocky rock systems, *ISRM*, Vol.2, 129-136.
- Harada, E., Goto, H., Sakai, T., & Ohno, M., 2002. 3-D Computational Model of Inter-Block Stress under a Failure of Precast Concrete Armor Units. *Journal of Japan Society of Civil Engineers*, 801-805 (in Japanese with English abstract).
- Japan Housing & Wood Technology Center, 2001. Manual for joining metallic fittings for timbered house, Tokyo.
- Johnson, K L., 1985. Contact mechanics, 2nd edn. Cambridge University Press.
- Architectural Institute of Japan, 1995. Design manual and explanation of timber structures, Architectural Institute of Japan (in Japanese).
- Kiyono, J., Miura, F., & Yagi, H., 1998. Simulation of evacuation behavior in a disaster by the Distinct Element Method. *Journal of the Japan Society of Civil Engineers*, **59**1, 366-378 (in Japanese with English abstract).
- Kiyono, J., Toki, K., Inukai, N., & Takeuchi, T., 2001. Evaluation of Safety on Evacuation Behavior from an Underground Space During an Earthquake, *Journal of the Japan Society of Civil Engineers*; **68**6/I-57, 31-43 (in Japanese with English abstract).
- Kiyono, Y. & Nagai, K., 2003. Earthquake-induced Train Accident and its Casualty Occurrence Mechanism. *Journal of Social Safety Science*, **5**: 1-10 (in Japanese with English abstract).
- Meguro, K. & Hakuno, M., 1994. Application of the Extended Distinct Element Method for Collapse Simulation of a Double-Deck Bridge. *Journal of Japan Society of Civil Engineers*, **48**3/I-26, 17-28, (in Japanese with English abstract).
- Ministry of Land, 2004, Infrastructure and Transport. Information of the Mid Niigata earthquake. <http://www.mlit.go.jp/chuetsujishin/> (in Japanese).
- Ohnishi, Y. & Kawano, M., 1986. Distinct Element Analysis of jointed Rock Mass Modeled by Voronoi Tessellation. *Journal of Japan Society of Civil Engineers*, **37**6/III-6, 231-239 (in Japanese with English abstract).